PERGAMON

International Journal of Multiphase Flow 28 (2002) 385–408

International Journal of Multiphase Flow

www.elsevier.com/locate/ijmulflow

Correlation of entrainment for annular flow in horizontal pipes

Lei Pan, Thomas J. Hanratty *

Department of Chemical Engineering, University of Illinois, 600 South Mathews Avenue, Urbana, IL 61801, USA

Received 11 January 2001; received in revised form 1 June 2001; accepted 3 October 2001

Abstract

Two correlations of measurements of entrainment for annular flow in horizontal pipes are presented for liquids with viscosities close to that of water. Entrainment is considered to result from a balance between the rate of atomization of the liquid layer flowing along the pipe wall and the rate of deposition of drops. At low gas velocities, gravitational settling controls the rate of deposition. At high gas velocities, droplet turbulence controls deposition. The first approach uses an empirical relation for entrainment in horizontal pipes at low gas velocities and an empirical relation for entrainment in vertical pipes at high gas velocities. The second uses a theoretical analysis for the rate of deposition that is valid both for high and low gas velocities. Present practice has been to use correlations that have been developed for vertical annular flows. They are faulty because they do not directly include the effects of gravitational settling.

Keywords: Gas–liquid pipe flow; Annular flow; Entrainment; Horizontal pipe

1. Introduction

Entrainment in annular flows is defined as the ratio of the mass flow of drops in the gas to the total mass flow of liquid, $E = W_{LE}/W_L$. An ability to predict E is critical to understanding the behavior of annular flows and to obtaining more reliable relations for liquid holdup and frictional pressure losses.

A theoretical approach in vertical flows involves the interpretation of entrainment as resulting from a balance of the rate of atomization of the liquid layer flowing along the wall, R_A, and the rate of deposition of drops, R_D. The following equation has been developed by Dallman et al.

* Corresponding author. Tel.: +1-217-333-1318; fax: +1-217-333-5052.
E-mail address: hanratty@scs.uiuc.edu (T.J. Hanratty).

0301-9322/02/$ - see front matter
PII: S0301-9322(01)00074-X

(1979), by Lopez de Bertodano and Assad (1997), Lopez de Bertodano et al. (1994), Schadel et al. (1990) and by Assad et al. (1998) to represent the rate of atomization for vertical systems with small liquid flows:

$$R_A = \frac{k'_A U_G^2 (\rho_G \rho_L)^{1/2}}{\sigma} \frac{(W_{LF} - W_{LFC})}{P}, \tag{1}$$

where W_{LFC} is the critical film flow below which atomization does not occur, P is the perimeter of the pipe, U_G is the gas velocity, σ is the surface tension, ρ_G is the gas density, ρ_L is the liquid density and $W_{LF} = W_L - W_{LE}$. The rate of deposition at small concentrations of drops is usually defined as being linearly dependent on the drop concentration

$$R_D = k_D C_B = k_D \left(\frac{W_{LE}}{Q_G S} \right), \tag{2}$$

where Q_G is the volumetric flow of gas, S is the ratio of the drop velocity to the gas velocity and C_B is the bulk concentration of drops.

For vertical flows, the following relation is derived for entrainment under the condition that $R_A = R_D$, provided the liquid viscosity is close to that for water:

$$\frac{(E/E_M)}{1 - (E/E_M)} = \frac{k'_A D U_G^3 S (\rho_G \rho_L)^{1/2}}{4 k_D \sigma}, \tag{3}$$

where k'_A is a dimensionless constant and the maximum entrainment, E_M, is given by

$$E_M = 1 - \frac{W_{LFC}}{W_L}. \tag{4}$$

An alternate formulation of Eq. (1) has been used for which U_G is replaced by $(U_G - U_{GC})$, where U_{GC} is the critical gas velocity below which no entrainment is observed. There is no physical reason for doing this in horizontal flows. In these cases, U_{GC} depends on gravitational settling; it is quite different from the critical gas velocity observed in vertical flows.

The implementation of Eqs. (3) and (4) for vertical flows requires the use of the theoretical result that k_D varies with the root-mean square of the velocity fluctuations in the direction of the wall, $(\overline{v_p^2})^{1/2}$. The relation of $(\overline{v_p^2})^{1/2}$ to system variables is complicated so, from the viewpoint of correlating data, the assumption has been made that U_G can be substituted for k_D/S. Data for air–water in vertical pipes with diameters of 2.54–5.72 cm are represented reasonably well with the equation

$$\frac{(E/E_M)}{1 - (E/E_M)} = A_1 \frac{D U_G^2 (\rho_G \rho_L)^{1/2}}{\sigma}. \tag{5}$$

Eqs. (3) and (5) are found to be useful over a much larger range of liquid flows than should be expected. The explanation for this is that the decreases of k'_A and k_D with increasing W_L tend to compensate.

This paper employs the approach outlined above to examine entrainment measurements in horizontal flows. Previous attempts to develop a correlation have involved the direct use of equations derived for vertical flows. The work of Dallman et al. (1984) is an example. Eq. (3) with $k'_A/k_D\sigma =$ constant had been used by Dallman et al. (1979) to correlate the measurements by

Cousins et al. (1965) of entrainment for air and water flowing upward in a 9.5 mm pipe (Dallman et al., 1979).

Therefore, this equation was an attractive choice to interpret their measurements of E for air and water flowing in horizontal 2.31 and 5.08 cm pipes, since it predicts maxima at large gas and liquid flows when measurements are made at several constant liquid rates or several constant gas rates. However, they found that Eq. (3) could not predict the stronger influence of gas velocity and the weaker influence of pipe diameter that was observed in horizontal flows. They, therefore, correlated their measurements by assuming

$$\frac{E/E_{\mathrm{M}}}{1-(E/E_{\mathrm{M}})} = f\left[\frac{k'_{\mathrm{A}} D U_{\mathrm{G}}^3 S(\rho_{\mathrm{G}}\rho_{\mathrm{L}})^{1/2}}{4k_{\mathrm{D}}\sigma}\right]. \tag{6}$$

This is, clearly, an empirical equation which has little chance to represent results for conditions different from those of the experiments from which it was derived.

Dallman et al. (1984) point out that Eq. (3) with $k'_{\mathrm{A}}/k_{\mathrm{D}}$ derived from experiments with vertical flows fails because this approach does not, directly, take account of the influence of gravitational settling on deposition. Williams et al. (1996) presented measurements of E for air and water flowing in a horizontal 9.53 cm pipe. These more clearly show the differences between the behavior of horizontal and vertical systems. The present paper is a continuation of the work of Williams et al., in that it introduces the effect of gravitational settling through a theoretical analysis of the relation of k_{D} to fluid turbulence and to gravitational settling (Lee et al., 1989a,b; Hay et al., 1996; Hanratty et al., 2000). The resulting predictive method represents a considerable advancement over the empirical correlation used by Dallman et al. (1984).

2. Entrainment equation for horizontal flows

In applying Eq. (3) to horizontal flows one needs to recognize that gravity causes an asymmetric distribution of drops in the gas phase and of the layer flowing along the wall. At large enough gas velocities, asymmetry disappears and one might expect that the equations for vertical flows would be applicable. (However, this condition is difficult to realize in most applications in large diameter pipes.) At low gas velocities, gravity becomes more important so asymmetries need to be taken into account. Gravitational settling can, also, increase k_{D} over what is observed for vertical flows. Consequently, the entrainment can be smaller and can be more strongly affected by gas velocity (since dropsize decreases with increasing gas velocity).

The approach employed by Williams et al. (1996) is to modify Eq. (3) so that it can be used for horizontal flows. The rate of atomization varies around the circumference. The assumption is made that the local rates are described by Eq. (1). If $\Gamma(\theta)$ equals the flow in the wall film per unit length at a given circumferential position, then the local rate of atomization is given as

$$R_{\mathrm{A}} = \frac{k'_{\mathrm{A}} U_{\mathrm{G}}^2 (\rho_{\mathrm{G}}\rho_{\mathrm{L}})^{1/2}}{\sigma}(\Gamma - \Gamma_{\mathrm{c}}) \tag{7}$$

if $\Gamma > \Gamma_{\mathrm{c}}$. For $\Gamma \leqslant \Gamma_{\mathrm{c}}$, the rate of atomization is zero. The average R_{A} around the circumference, defined by

$$\langle R_A \rangle = \frac{1}{\pi D} \int_0^{\pi} D R_A \, d\theta, \tag{8}$$

is given as

$$\langle R_A \rangle = \frac{k'_A U_G^2 (\rho_G \rho_L)^{1/2}}{\sigma} \left[\frac{W_{LF}}{P} - \Gamma_c^* \right], \tag{9}$$

where

$$\Gamma_c^* = \Gamma_c - \frac{1}{\pi} \int_{\theta_c}^{\pi} (\Gamma_c - \Gamma) \, d\theta. \tag{10}$$

Here, θ_c is the angular location at which $\Gamma = \Gamma_c$. If $\Gamma > \Gamma_c$ around the whole circumference $\theta_c = \pi$ and $\Gamma_c^* = \Gamma$. If $\Gamma < \Gamma_c$ over a portion of the circumference from θ_c to π, then $\Gamma_c^* < \Gamma$.

Measurements of concentration profiles of drops in vertical flows (Hay et al., 1996) reveal that, under fully developed conditions, the concentration is uniform over the pipe cross-section so that the bulk concentration equals the concentration at the wall. This is not the case for horizontal flows. The local rate of deposition is, therefore, represented as

$$R_D = k_D \left(\frac{C_W}{C_B} \right) C_B = k_D \frac{C_W}{C_B} \left(\frac{W_{LE}}{Q_G S} \right), \tag{11}$$

where horizontal flows R_D, k_D and C_W vary around the pipe circumference. Therefore, the spatially averaged R_D is given as

$$\langle R_D \rangle = \left\langle k_D \frac{C_W}{C_B} \right\rangle \frac{W_{LE}}{Q_G S}. \tag{12}$$

Under fully developed conditions $\langle R_A \rangle = \langle R_D \rangle$. The following equation, analogous to Eq. (3), can be developed:

$$\frac{(E/E_M)}{1 - (E/E_M)} = \frac{k'_A D U_G^3 S (\rho_L \rho_G)^{1/2}}{4 \langle k_D (C_W/C_B) \rangle \sigma}, \tag{13}$$

where

$$E_M = 1 - \frac{\pi D \Gamma_c^*}{W_L}. \tag{14}$$

For low viscosity liquids the initiation atomization occurs when disturbance waves appear on the liquid layer. Measurements of Andreussi et al. (1985) of the liquid flow needed to initiate disturbance waves in vertical flows can be used to calculate the critical flow per unit length, $\Gamma_c = W_{LFC}/\pi D$. These are represented by the following equation:

$$Re_{LFC} = 7.30(\log_{10} \omega)^3 + 44.2(\log_{10} \omega)^2 - 263(\log_{10} \omega) + 439, \tag{15}$$

where

$$Re_{LFC} = \frac{4\Gamma_c}{\mu_L}, \tag{16}$$

$$\omega = \frac{\mu_L}{\mu_G} \sqrt{\frac{\rho_G}{\rho_L}}. \tag{17}$$

For air and water at standard conditions, $\omega = 1.861$ and $Re_{LFC} = 370$. Measurements in horizontal flows by Dallman (1978) and by Laurinat (1982) show larger values of Γ_c by a factor of about 1.3, probably because of the asymmetry of the liquid layer. A general relation representing their results is not available, so Eq. (16) is used in the calculations presented in this paper.

Eq. (15) was derived from measurements for $\omega = 1.8$ to 28. It should not be used outside this range. For large μ_L (or large ω) disturbance waves no longer exist on the film so Eq. (15) would not describe a critical liquid flow. In fact, Eq. (1) probably cannot be used to represent the rate of atomization at large μ_L (see the paper by Hoogendorn and Welling, 1979, which suggests that R_A varies as W_{LF}^2).

Eq. (13) will be used to interpret experimental results. Section 3 summarizes available data and develops an empirical correlation which accounts for the effect of gravitational settling. Section 4 incorporates recently available theoretical results on k_D into Eq. (13). Section 5 compares theoretical calculations of entrainment with available data. Section 6 uses theoretical and empirical correlations, developed with the help of measurements for air and water flowing in pipes with diameters of 2.31, 5.08 and 9.53 cm, to predict entrainment in a horizontal natural gas pipeline. The conditions in this system are quite different from what is found for air and water flowing under atmospheric conditions. The gas density is larger; the surface tension is smaller; the pipe diameter is larger. Unfortunately, we do not have, at our disposal, data to test the predictions. The merit of doing this calculation is that it illustrates how one can utilize available knowledge about entrainment.

The results presented in this paper are a best guess at an approach which can have general usage. We do not consider it to be final because of the limited amount of information that is used. One can expect the approach to be amended with the availability of a better understanding of the droplet exchange process, of dropsizes, of the effect of gravity on the distribution of the liquid phase, and of the effect of fluid properties.

3. Experimental results

3.1. Correlating equations

Measurements by Williams (1986), Laurinat (1982), Dallman (1978) and by Paras and Karabelas (1991) are summarized in Table 1. They are for the air–water system and cover pipe diameters of 2.31–9.53 cm, gas velocities of 11–131 m/s and gas densities of 1.26–2.75 kg/m^3.

These measurements were carried out at low enough gas velocities that gravitational settling is a major contributor to deposition. Therefore, for the purpose of examining the influence of system variables on entrainment, Eq. (13) is simplified by substituting the terminal velocity, u_T, for $\langle k_D(C_W/C_B)\rangle$ and by taking S as constant; i.e.,

$$\frac{(E/E_M)}{1-(E/E_M)} = A_2\left(\frac{DU_G^3\rho_L^{1/2}\rho_G^{1/2}}{\sigma u_T}\right). \tag{18}$$

The use of Eq. (18), therefore, presumes a large value of $u_T/(\overline{v_p^2})^{1/2}$.

Table 1
Experiments that are used

	Williams (1986, 1990)	Laurinat (1982)	Dallman (1978)	Paras and Karabelas (1991)
Fluids	Air–water	Air–water	Air–water	Air–water
D (cm)	9.53	5.08	2.31	5.08
U_G (m/s)	26–88	11–131	15–88	31–67
W_L (kg/s)	0.12–0.86	0.033–0.97	0.003–0.25	0.04–0.39
ρ_G (kg/m^3)	1.3–1.85	2.05	1.26–2.75	1.3–2.3
No. of runs	29	52	114	17

The terminal velocity for a spherical drop is given as

$$u_T^2 = \frac{4dg\rho_L}{3C_D\rho_G}, \tag{19}$$

where d is the drop diameter and C_D is the drag-coefficient, given as

$$C_D \sim Re_p^{-m} \tag{20}$$

with $Re_p = du_T\rho_G/\mu_G$. For Newton's law $m = 0$. For Stokes law $m = 1$ and

$$C_D = \frac{24}{Re_p}. \tag{21}$$

For $1.92 \leqslant Re_p < 500$, m can be approximated as 0.6; i.e.,

$$C_D = \frac{18.5}{Re_p^{0.6}}. \tag{22}$$

The substitution of Eqs. (19) and (20) into Eq. (18) gives

$$\frac{(E/E_M)}{1-(E/E_M)} = A_2\left(\frac{DU_G^3\rho_L^{0.5}\rho_G^{0.5}}{\sigma}\right)\left(\frac{\rho_G^{1-m}\mu_G^m}{d^{1+m}g\rho_L}\right)^{1/(2-m)}. \tag{23}$$

3.2. Evaluation of the drop size

Measurements of drop size, d, in horizontal gas–liquid flows are sparse, so results for vertical configurations were used. A first guess might be that $\rho_G U_G^2 d/\sigma$ is a constant. However, experiments show that d varies roughly as U_G^{-1}, rather than U_G^{-2}.

Tatterson et al. (1977) have provided a theory which suggests that

$$\left(\frac{\rho_G U_G^2 d}{\sigma}\right)\left(\frac{d}{\lambda}\right) = \text{constant}, \tag{24}$$

where λ is the wavelength of the waves that produces the drops. This result suggests the following equations which give $d \sim U_G^{-1}$:

$$\left(\frac{\rho_G U_G^2 d_{32}}{\sigma}\right)\left(\frac{d_{32}}{D}\right) = 0.0091 \tag{25}$$

and

$$\left(\frac{\rho_G U_G^2 d_{32}}{\sigma}\right)\left(\frac{d_{32}}{\lambda_A}\right) = 0.14, \tag{26}$$

where λ_A is a length scale defined by Azzopardi (1985) as

$$\lambda_A = \left(\frac{\sigma}{\rho_L g}\right)^{0.5}. \tag{27}$$

Annular flows contain a distribution of drop sizes. The Sauter-mean diameter, d_{32}, is representative of the size of the larger drops that contain most of the volume (see Tatterson et al., 1977). Eq. (25) differs from Eq. (26), in that it states that d_{32} increases with pipe diameter.

The constants on the right-hand sides of Eqs. (25) and (26) were specified by considering the measurements of Hay et al. (1996) for air and water flowing in a vertical pipe. These are close to a correlation presented by Azzopardi (1985).

3.3. Effect of liquid flow, W_L

Williams measured entrainment by determining local droplet fluxes with a sampling tube, and integrating over the space occupied by the gas (cf. Williams et al., 1996; Williams, 1986; Williams, 1990). The system was air–water flowing at atmospheric pressure in a horizontal pipe with a diameter of 9.53 cm. The results are presented in Fig. 1 as a plot of E/E_M versus W_L, with gas

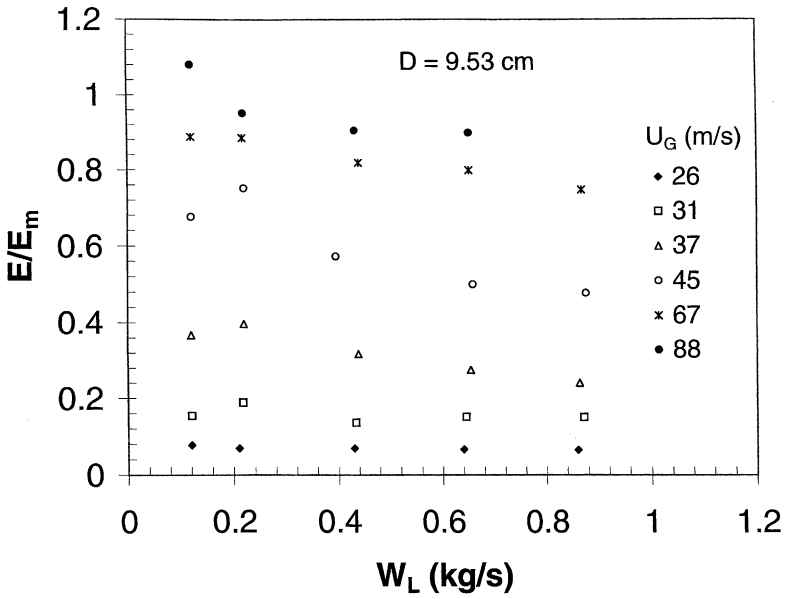

Fig. 1. Measurements of E/E_M obtained by Williams (1986, 1990) for air and water flowing in a horizontal pipe.

velocity as a parameter. In calculating E_M, the term Γ_c^* was set equal to Γ_c. A value of $W_{LFC} = 0.025$ kg/s was obtained from Eq. (15). The main feature of Fig. 1 is that E/E_M is weakly dependent on liquid flow and strongly affected by gas velocity, as predicted by Eq. (13). The extrapolation of these results to $E = 0$ gives a rough estimate of a critical gas velocity of $U_{GC} \cong 21$ m/s.

The explanation of the effects of W_L, that are observed, is complicated. For example, the drop in E at large W_L for $U_G = 45$ and 67 m/s has been suggested by Williams et al. (1996) to be due to a decrease in k'_A at large W_{LF}. Another explanation is the existence of secondary flows in the gas at large liquid flows in this range of gas velocities (Dykhno et al., 1994). These could increase the rate of deposition and, therefore, decrease the entrainment. Observed changes of E/E_M with changes in W_L could also result from experimental error associated with the methods used to obtain the total droplet flux from measured local values at a limited number of positions.

In studies in a 2.31 cm pipe (Dallman, 1978) and in a 5.08 cm pipe (Laurinat, 1982; Laurinat et al., 1984) the flow of the liquid wall layer was measured by withdrawing it through a porous wall. The entrainment is obtained by subtracting the measured W_{LF} from W_L. This is a more difficult measurement in horizontal flows than in vertical flows because the wall layer is distributed asymmetrically and because it can be quite thick at the bottom of the pipe. At low W_L, close to W_{LFC}, this technique provides erratic results. At very large W_{LF} the complete removal of the liquid from the wall is very difficult.

Results obtained in 2.31 and 5.08 cm pipes are similar to what is found for a 9.53 cm pipe, in that measured E/E_M are much more sensitive to changes in the flow of the gas than to changes in the flow of the liquid. There also is a tendency for E/E_M to decrease for large W_L at intermediate gas velocities. This behavior is somewhat stronger than what is observed for a pipe with $D = 9.53$ cm. A rough estimate of a critical gas velocity of 15 m/s is obtained for 2.31 and 5.08 cm pipes.

An important factor in understanding measurements of entrainment is the asymmetrical distribution of the liquid. Fig. 2(a) gives plots of the ratio of the height of the wall layer at the bottom of the pipe, m_{bot}, to the average height around the circumference for the experiments represented in Fig. 1 (Williams, 1990). A striking aspect of these results is the increase in asymmetry with decreasing U_G or decreasing $U_G/(gD)^{0.5}$. At $U_G = 88$ m/s the layer is close to being uniformly distributed in a 9.53 cm pipe. For $U_G = 31$ and 37 m/s, the flow is highly asymmetric so gravity is having a very strong effect. Values of $m_{bot}/\langle m \rangle$ measured by Dallman (1978) and by Laurinat (1982) for air and water flowing in 2.31 and 5.08 cm pipes are given in Figs. 2(b) and (c).

3.4. Effect of gas velocity U_G and the definition of $\langle E/E_M \rangle$

At present, it is not possible to provide an explanation for the observed effects of W_L on E/E_M. Therefore, measured values, for different liquid flows, at a given U_G were averaged and a correlation that represents the effect of gas velocity on this average was sought. In doing this, values of E/E_M determined at W_L close to W_{LFC} were ignored, because of concern over their accuracy. Table 2 summarizes the $\langle E/E_M \rangle$ obtained in this way. The W_L given in the table represent the midrange over which the average E/E_M was calculated for a given U_G. This procedure greatly reduces the number of test runs that are directly used, but it allows a clearer definition of the effect of gas velocity.

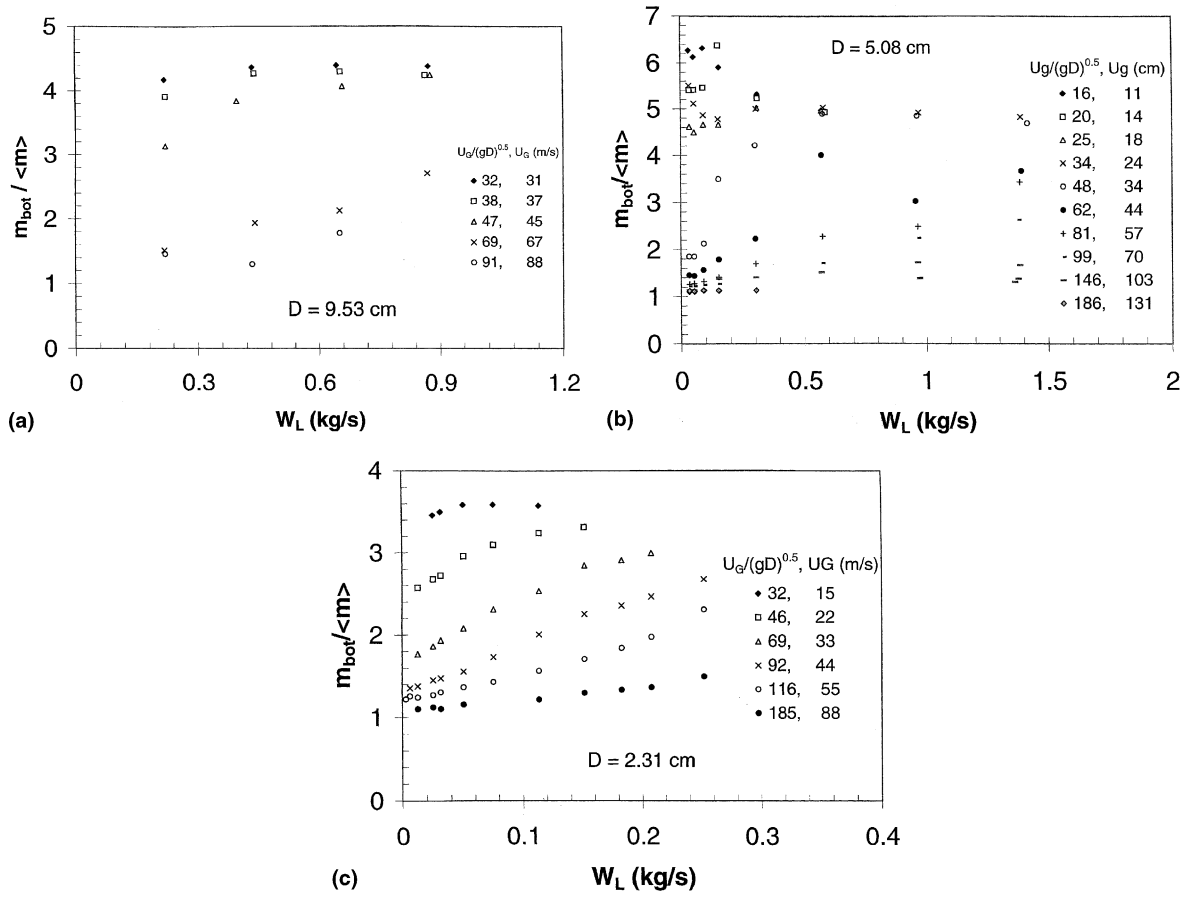

Fig. 2. Measurements of the ratio of the liquid height at the bottom of the pipe to the average liquid height: (a) air–water in a horizontal pipe with $D = 9.53$ cm; (b) air–water, with $D = 5.08$ cm; (c) air–water, with $D = 2.31$ cm.

Table 2
Values of $\langle E/E_m \rangle$ = the average E/E_M for different liquid flows

$W_L = 0.64$ kg/s (Williams, 1990)		$W_L = 0.31$ kg/s (Laurinat, 1982)		$W_L = 0.1134$ kg/s (Dallman, 1978)		$W_L = 0.3$ kg/s (Paras and Karabelas, 1991)	
U_G (m/s)	$\langle E/E_M \rangle$	U_G (m/s)	$\langle E/E_M \rangle$	U_G (m/s)	$\langle E/E_M \rangle$	U_G (m/s)	$\langle E/E_M \rangle$
26	0.068	18	0.064	15	0.04	31	0.24
31	0.15	24	0.24	22	0.098	45	0.75
37	0.3	34	0.56	33	0.36	48	0.86
45	0.54	44	0.7	44	0.72		
67	0.815	57	0.9	55	0.88		
88	0.9	70	ca. 1	88	ca. 1		
		103	ca. 1				
		131	ca. 1				

Figs. 3(a) and (b) compare values of E calculated from the $\langle E/E_M \rangle$ listed in Table 2 with measurements of E in a 9.53 cm pipe and in a 2.31 cm pipe. The maximum entrainments were calculated with (4) using a W_{LFC} obtained from Eq. (15) and the values of W_L listed in Table 2. The characterization of the measurements in terms of $\langle E/E_M \rangle$ as a function of U_G does a good job of representing the data, except for W_L close to W_{LFC}. The erratic behavior close to W_{LFC} could be due, partially, to the use of a constant for Γ_c^*, rather than Eq. (10).

Values of $E/E_M/1-(E/E_M)$ for 9.53, 5.08 and 2.31 cm pipes are plotted in Fig. 4 versus $\rho_G^{0.5} U_G$, where ρ_G is the gas density that prevailed in the experiments represented by that data point. The E/E_M are the averages for a given gas velocity, defined above and presented in Table 2. Two sets

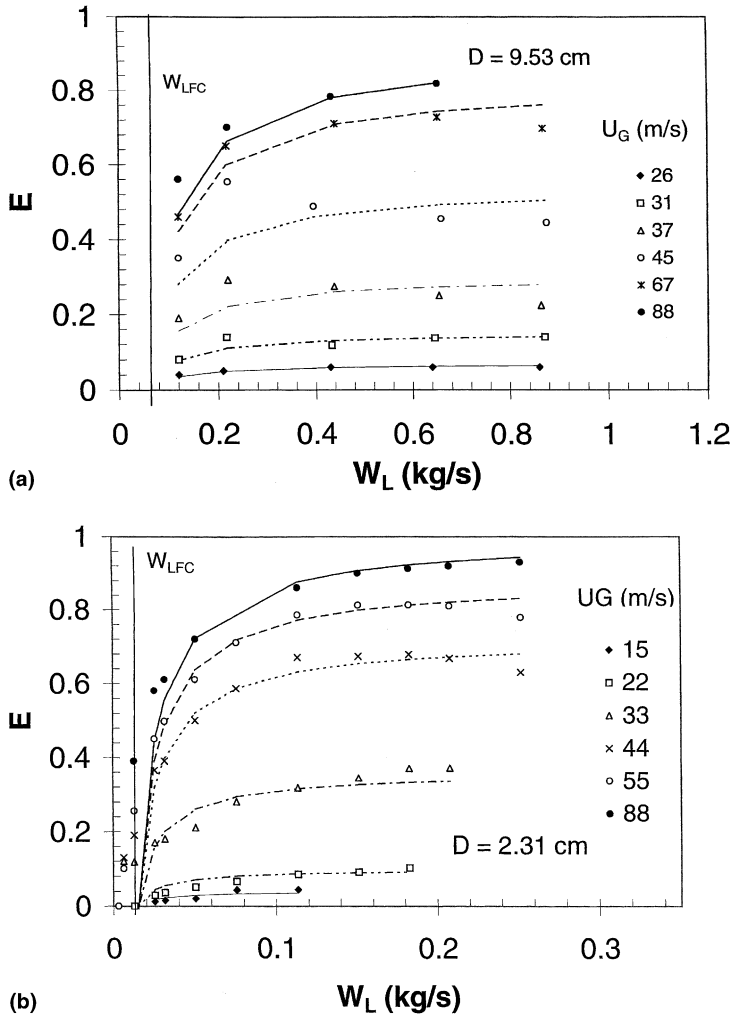

Fig. 3. Values of E calculated from $\langle E/E_M \rangle$ = average of E/E_M for a number of liquid flows (listed in Table 2): (a) $D = 9.53$ cm; (b) $D = 2.31$ cm.

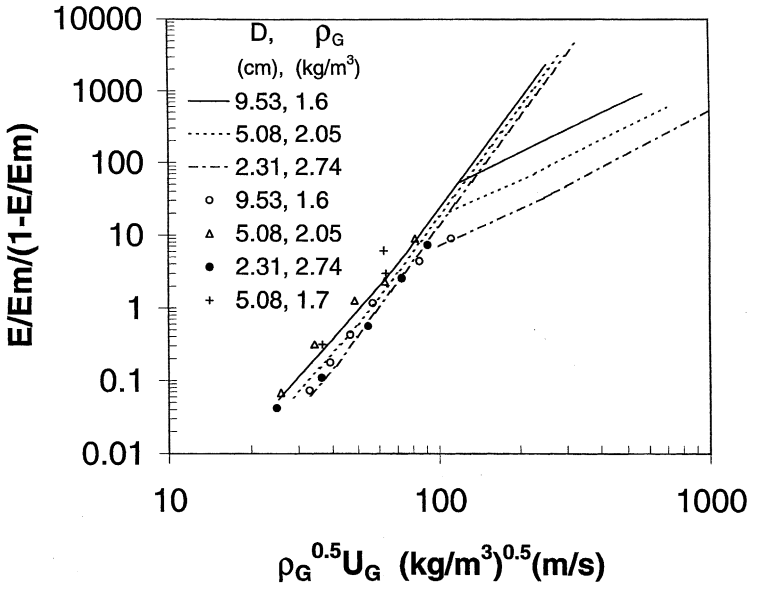

Fig. 4. Comparison of measurements of $(E/E_M)/1-(E/E_M)$ with empirical equation (18) and d_{32} given by Eq. (25). The data points are the averages for a number of liquid flows given in Table 2.

of data for a 5.08 cm pipe are presented. One was obtained by Laurinat (1982) and the other, by Paras and Karabelas (1991). The three lines going through the data were calculated with Eq. (18) for $D = 9.53$, 5.08, 2.31 cm, using $A_2 = 9 \times 10^{-8}$ and the values of ρ_G listed in the figure. The drop sizes, needed to calculate u_T, are the d_{32} defined by Eq. (25). These roughly vary as U_G^{-1}. If Stokes law is used ($m = 1$), the right-hand side of Eq. (23) gives $(E/E_M)/1-(E/E_M)$ varying as U_G^5. An intermediate behavior for C_D ($m = 0.6$) gives a dependency of $U_G^{4.2}$. The change in slope of the lines calculated from Eq. (18) represents a change from Stokes law at large U_G to the intermediate relation for C_D at small U_G.

The three lines at the top part of Fig. 4 represent the entrainment that would be observed for gas–liquid flow in vertical tubes. They were calculated with Eq. (5), using $A_1 = 8.8 \times 10^{-5}$. This value is suggested from the theoretical calculations presented in Section 7. The important point to be made in comparing these lines with the data in Fig. 4 is that correlations based on results in vertical pipes will overpredict the entrainment and will not capture the strong influence of gas velocity observed in horizontal pipes.

The favorable comparison of the results with Eq. (18) indicates that the influence of gravitational settling needs to be considered in order to capture the influence of gas velocity at small gas velocities. For very large gas velocities the drops should be uniformly distributed and entrainment should be described by equations developed for vertical pipes. However, under these circumstances, E/E_M is close to unity.

The results in Figs. 2(a)–(c) for the air–water system show that the high velocity asymptotic behavior should be approached for $U_G/(gD)^{0.5}$ approximately equal to 190, that is at gas velocities of 90–180 m/s as D varies from 2.31 to 9.53 cm.

3.5. Effect of pipe diameter

The measurements in Fig. 4 suggest a weak dependency of $(E/E_M)/1-(E/E_M)$ on pipe diameter when comparisons are made at the same value of the E/E_M and the data are plotted against $\rho_G^{0.5}U_G$. They indicate a decrease in the value of $\rho_G^{0.5}U_G$ is needed to maintain a given level of entrainment with a change of D from 2.3 to 5.08 cm and an increase, with a change from 5.08 to 9.53 cm. The results for $D=2.31$ and 5.08 cm are the same. However, the use of $\rho_G^{0.5}$ in the abscissa is not based on any theoretical arguments. The apparent effect of pipe diameter, therefore, depends on the exponent that is chosen for ρ_G. For example, as can be seen from Table 2, a different trend would be observed if only U_G were used as the abscissa. The data for $D=2.31$ cm and $D=5.08$ cm would then be closer together and larger values of U_G would be needed to obtain the same E/E_M for $D=9.53$ cm.

The influence of pipe diameter in Eq. (18) comes from the appearance of D in the numerator and the dependency of u_T on D. Eqs. (18) and (23) give $(E/E_M)/1-(E/E_M)$ varying with $D/d^{1.1}$ if C_D is in the intermediate range and with D/d^2 if C_D is given by Stokes law. If d is independent of pipe diameter (Eq. (26)) a stronger effect of D than shown in Fig. 4 is predicted with Eq. (18). The lines in Fig. 4 were obtained by using Eq. (25), which gives d increasing as $D^{1/2}$. Eqs. (18) and (23) then predict an insensitivity to D seen in the experimental data. One could conclude, from the comparisons of Eq. (18) with the data, that drop size increases with D, as predicted by Eq. (25). This might not be warranted because the substitution of u_T for $\langle k_D(C_W/C_B)\rangle$ in Eq. (13) is an oversimplification.

Because of the strong effect of gas velocity on E/E_M a greater sensitivity to changes in pipe diameter is seen if comparisons of measured E/E_M are made at the same value of $\rho_G^{0.5}U_G$ so, in this context, the development of a sound theoretical understanding of the effects of D and ρ_G is critically important. This theory needs to take into account the asymmetric distribution of liquid, which increases with increasing D, and to have a correct representation of the drop size.

4. Theoretical approach

4.1. Prediction of k_D

The local rate of deposition at a given circumferential location, in the units of mass per unit time per unit area, may be described as the product of the average velocity of drops in the direction of the wall, V_W, and the concentration of drops at the wall, in the units of mass per unit volume.

$$R_D = V_W C_W. \tag{28}$$

A comparison with Eq. (11) defines k_D as equal to V_W. The variation of k_D with θ is, therefore, described by the variation of V_W because of gravitational effects.

A simplifying assumption is that the drops have come to a stationary state with the fluid turbulence. Their velocities would, then, have a mean value in the radial direction, $u_T\cos\theta$, due to gravitational settling. Here, $\theta=0$ is at the bottom of the pipe where the mean velocity equals u_T. At the top of the pipe, it equals $-u_T$.

The droplets start their free-flight to the wall from outside the viscous wall layer, so the non-homogeneities in the fluid turbulence close to the boundary can be ignored. The distribution of the velocity fluctuations in a direction normal to the wall is assumed to be Gaussian, so that

$$p(x) = \frac{1}{(2\pi)^{1/2}\sigma_p} \exp\left[-\frac{(x-\mu)^2}{2\sigma_p^2}\right], \tag{29}$$

where $x = \mu + v_p$, $\sigma_p = (\overline{v_p^2})^{1/2}$. For a vertical flow, $\mu = 0$; for a horizontal flow, $\mu = u_T \cos\theta$. The local $k_D(\theta)$ is then given as

$$k_D(\theta) = V_W = \int_0^\infty x p(x)\,dx. \tag{30}$$

By substituting Eq. (28) into Eq. (29) one obtains

$$\begin{aligned} V_W &= \int_{x=0}^{x=\infty} \frac{(x-\mu)}{\sqrt{2\pi}\sigma} \exp\left[-\frac{(x-\mu)^2}{2\sigma_p^2}\right] dx + \int_{x=0}^{x=\infty} \frac{\mu}{\sqrt{2\pi}\sigma_p} \exp\left[\frac{-(x-\mu)^2}{2\sigma_p^2}\right] dx \\ &= \int_{-\mu}^{\infty} \frac{z}{\sqrt{2\pi}\sigma_p} \exp\left[\frac{-z^2}{2\sigma_p^2}\right] dz + \int_{-\mu}^{\infty} \frac{\mu}{\sqrt{2\pi}\sigma_p} \exp\left[\frac{-z^2}{2\sigma_p^2}\right] dz. \end{aligned} \tag{31}$$

The integral in Eq. (31) considers only positive values of $x = \mu + v_p$. An integration from $-\infty$ to $+\infty$ gives $V_W = \mu$. When $(u_T/\sigma_p) \to 0$. Eq. (31) gives

$$V_W = \left(\frac{\sigma_p^2}{2\pi}\right)^{0.5} \tag{32}$$

so that only particle turbulence is responsible for deposition. For $(u_T/\sigma_p) \to \infty$,

$$V_W = u_T \cos\theta, \tag{33}$$

so that gravitational settling is controlling deposition. Eq. (31) gives $k_D/(\sigma_p^2/2\pi)^{0.5}$ as a function of $\psi = u_T \cos\theta/\sigma_p$. This result is plotted in Fig. 5. An expression for $\overline{v_p^2}$ is needed in order to use Eq. (31) or Fig. 5.

4.2. Evaluation of $\sigma_p^2 = \overline{v_p^2}$

The turbulent motion of the drops is caused by fluid velocity fluctuations. The ability of the drops to respond to fluid turbulence is represented by the reciprocal of the inertial time constant, β. For drops in the Stokesian range

$$\beta = \frac{18\mu_G}{d^2\rho_L} \tag{34}$$

and

$$u_T = \frac{d^2 g(\rho_L - \rho_G)}{18\mu_G}. \tag{35}$$

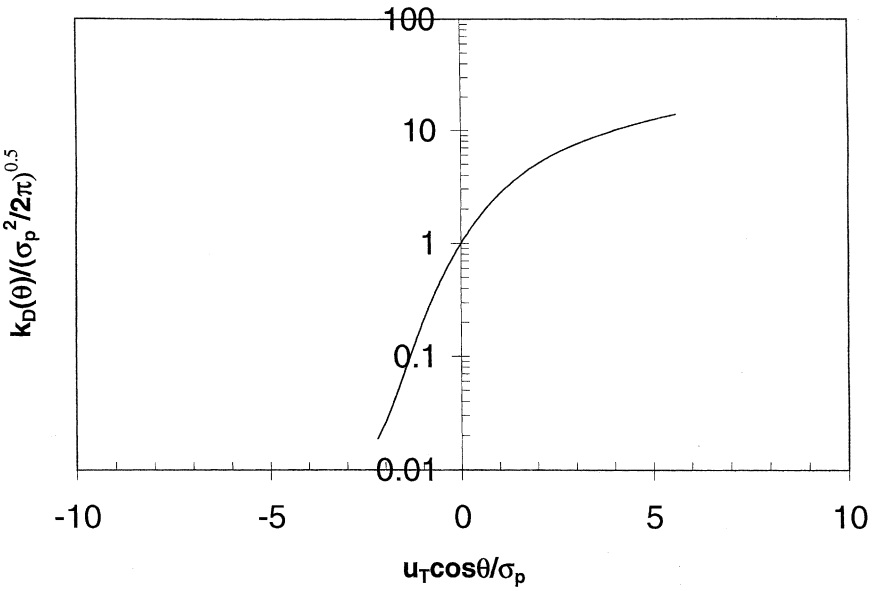

Fig. 5. Plot of $V_W/(\sigma_p^2/2\pi)^{0.5}$ versus $\varphi = u_T \cos\theta/\sigma_p$.

In general,

$$\beta = \frac{3C_D\rho_G u_T}{4d\rho_L}, \tag{36}$$

where the average slip between the gas and the drops is set equal to the terminal velocity. For the intermediate range of C_D, where Eq. (22) is valid,

$$u_T = \frac{d^{1.6}g(\rho_L - \rho_G)}{13.9\rho_G^{0.4}\mu_G^{0.6}}. \tag{37}$$

Measurements by Lee et al. (1989a,b), for dilute concentrations of drops and for situations in which the drops have come into equilibrium with the fluid turbulence, give

$$\overline{v_p^2} = \left(\frac{\beta\tau_{LF}}{0.7 + \beta\tau_{LF}}\right)\overline{v_G^2}, \tag{38}$$

where τ_{LF} is the Lagrangian time constant characterizing the fluid turbulence and $\overline{v_G^2} = \sigma_G^2$ is the mean-square of the velocity fluctuations of the gas in a direction normal to the wall. The gas-phase turbulence is given by

$$\sigma_G^2 = (0.9v^*)^2, \tag{39}$$

where v^* is the friction velocity

$$v^* = (\tau_i/\rho_G)^{0.5} = U_G(f_i/2)^{0.5}. \tag{40}$$

The Lagrangian time constant of the gas-phase turbulence can be approximated as (Hay et al., 1996)

$$\tau_{LF} = \frac{0.046D}{v^*}. \tag{41}$$

For situations in which τ_{LF} is large enough compared to the inertial time constant of the fluid (large $\beta\tau_{LF}$) the particles follow the fluid turbulence and $\sigma_p = \sigma_G$. For very small $\beta\tau_{LF}$ the particle turbulence is less than the fluid turbulence

$$\overline{v_p^2} = \frac{\beta\tau_{LF}\overline{v_G^2}}{0.7}. \tag{42}$$

Annular flows are usually characterized by $\beta\tau_{LF} \cong 0.1$ so that $\overline{v_p^2} \cong \frac{1}{7}\overline{v_G^2}$.

The interfacial friction factors needed to evaluate v^* are approximated by a relation suggested by Dallman et al. (1979) for horizontal flows:

$$\frac{f_i}{f_s} = \left[1 + (61F^{0.5})^2\right]^{0.5}, \tag{43}$$

$$F = \frac{\mu_L \rho_G^{0.5} \gamma(Re_{LF})}{\mu_G \rho_L^{0.5} Re_G^{0.9}}, \tag{44}$$

$$\gamma = \left[\left(0.5Re_{LF}^{0.5}\right)^3 + \left(0.028Re_{LF}^{0.9}\right)^3\right]^{1/3}, \tag{45}$$

$$\begin{aligned} f_s &= 0.046\left(\frac{4W_G}{\pi D\mu_G}\right)^{0.2}, \\ Re_{LF} &= \frac{4W_{LF}}{\pi D\mu_L} = \frac{4(1-E)W_L}{\pi D\mu_L}. \end{aligned} \tag{46}$$

4.3. Drop size distribution

The upper-limit, log-normal distribution used by Mugele and Evans (1951) and Wicks and Dukler (1960) was chosen to represent the distribution of drop sizes. Define the product of f_v and dd_p as the fraction of the total volume contributed by drops with diameters between d_p and $d_p + dd_p$.

$$f_v = \frac{\delta d_p}{\sqrt{\pi} d_p (d_m - d_p)} \exp\left[-\delta^2\left(-\delta^2 \ln\frac{d_p}{d_m - d_p} - \ln\frac{d_{v\mu}}{d_m - d_{v\mu}}\right)\right]. \tag{47}$$

Parameters d_m and $d_{v\mu}$, respectively, designate the maximum and the volume-median drop size. The suggestions of Tatterson et al. (1977) are followed by using $\delta = 0.84$ and $(d_m/d_{v\mu}) = 3.6$. The volume-median diameter is related to the more commonly used Sauter-mean diameter with the equation

$$d_{v\mu} = \frac{d_{32}}{0.765} \tag{48}$$

if $\delta = 0.84$ and $(d_m/d_{v\mu}) = 3.6$.

4.4. Concentration profiles of droplets

The specification of $C_W(\theta)$ in Eq. (13) requires the development of an equation for the concentration profile. Measurements by Williams (1986) and by Paras and Karabelas (1991) show that the concentration of drops is approximately uniform in planes perpendicular to the direction of gravity. The determination of $C_W(\theta)$, then, requires only a calculation of $C(y)$, where y is the vertical axis. The method used by Paras and Karabelas is followed.

A mass balance gives

$$\frac{d(u_T C)}{dy} + \frac{d(\varepsilon \frac{dC}{dy})}{dy} + \frac{2(R_A - R_D)}{D \sin^2 \theta} = 0, \tag{49}$$

where ε is turbulent diffusivity of the drops. The equation indicates that gravitational settling is opposed by turbulent diffusion. The third term represents a source or sink of drops at the boundary. Integration of Eq. (49) gives

$$\varepsilon \frac{dC}{dy} + u_T C + D \int \frac{R_A - R_D}{(D/2)^2 - y^2} dy + B = 0, \tag{50}$$

which can be written as

$$\varepsilon \frac{dC}{dy} + u_T C = a(y), \tag{51}$$

$$a(y) = -D \int \frac{R_A - R_D}{(D/2)^2 - y^2} - B. \tag{52}$$

The evaluation of Eq. (52) requires a knowledge of local values of R_D and R_A. This complicates the analysis, so the simplification is made that the influence of $a(y)$ can be ignored.

The integration of Eq. (51) with $a(y) = 0$ and $\varepsilon =$ constant gives

$$C = C_0 \exp\left(-\frac{u_T}{\varepsilon} y\right) \tag{53}$$

with C_0 being the concentration at the bottom of the pipe, $y = 0$. Paras and Karabelas (1991) suggest that $\varepsilon = \varsigma(D/2)v^*$. However, a comparison of Eq. (53) with the experiments of Paras and Karabelas in a 5.08 cm pipe and of Williams in a 9.53 cm pipe shows that ς needs to vary with pipe diameter if $a(y)$ is assumed to be zero and if the above relation is used for ε. Clearly, the use of Eq. (53) must be regarded as a rough empirical fit to the data.

Figs. 6(a) and (b) show how the measurements of Williams and of Paras and Karabelas are represented by Eq. (53) by, respectively, using $\varsigma = 0.04$ and $\varsigma = 0.08$. More work needs to be done in which non-constant values of ε and non-zero values of $(R_A - R_D)$ are used in Eq. (49).

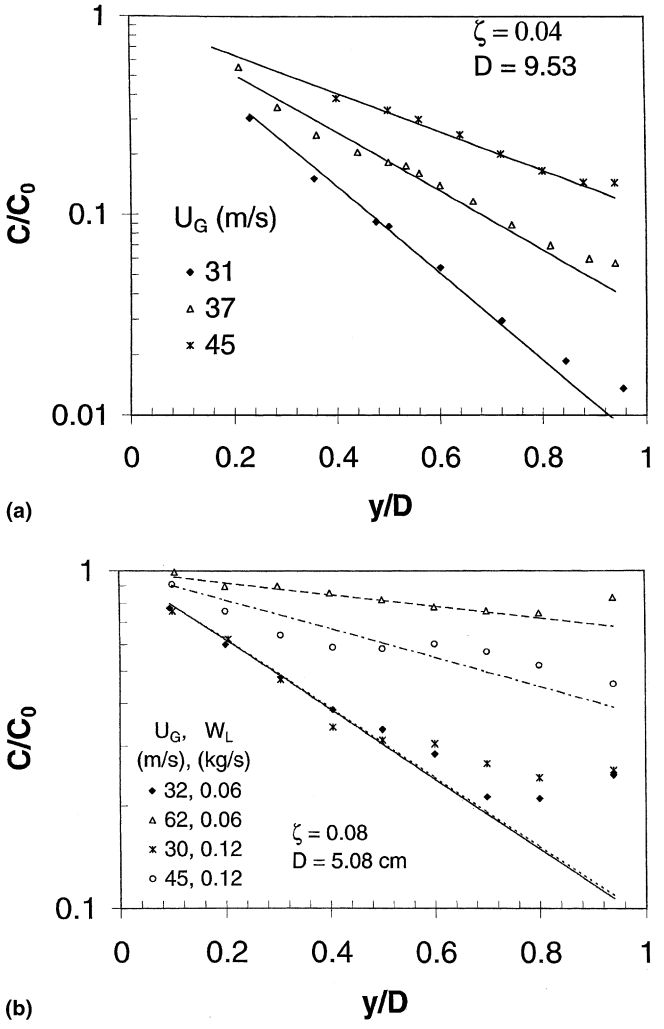

Fig. 6. Comparison of measurements of spatial distribution of drops distribution with Eq. (53) for air–water flows: (a) $D = 9.53$ cm; (b) $D = 5.08$ cm.

5. Theoretical calculations

Eq. (13) will be compared with measurements by using the theoretical relations for k_D and the empirical relations for C_W/C_B developed in Section 4. The constant k'_A is selected empirically. The term to be evaluated is

$$\left\langle k_D \frac{C_W}{C_B} \right\rangle = \frac{1}{\pi} \int_0^{\pi} k_{D\theta} \left(\frac{C_W}{C_B} \right) d\theta, \tag{54}$$

where θ is the angle measured from the bottom of the pipe and the distance from the bottom is given as

$$y = R(1 - \cos\theta) \tag{55}$$

with R equal to the radius of the pipe. The concentration at the wall, $C_W(\theta)$, is then given by (53) and C_W/C_B is calculated as

$$\frac{C_W}{C_B} = \frac{\exp(-yu_T/\varepsilon)}{(2/\pi)\int_0^{\pi}[\exp(-yu_T/\varepsilon)](\sin\theta)\,d\theta} \tag{56}$$

with y given by Eq. (55), and $\varepsilon = -(D/2)v^*\varsigma$. Eq. (54) is then evaluated by substituting Eqs. (56) and (30). It is noted that $k_D(\theta)$ varies with σ_p^2 and $\psi = u_T\cos/\sigma_p$. The influence of drop size enters into the evaluation of u_T and of σ_p. Smaller drops have smaller u_T and larger σ_p.

Two approaches could be taken: The behavior of the drops could be described by assuming they have a constant diameter equal to d_{32}, as was done in developing an empirical relation. The second choice is to take account of the distribution of drop sizes in a direct way

$$\left\langle k_D\frac{C_W}{C_B}\right\rangle = \int_0^{d_m} k_{D\theta}\frac{C_W}{C_B}f_v\,dd_p, \tag{57}$$

where f_v is given by Eq. (47).

A comparison of calculated and measured E/E_M is presented in Fig. 7(a) for air–water flow in pipes with diameters of 2.31, 5.08 and 9.53 cm. Eq. (53) was used in the calculations, with $\varsigma = 0.08$ for the 2.31 and the 5.08 cm pipes and with $\varsigma = 0.04$ for the 9.53 cm pipe. The distribution of drop sizes is taken into account and a value of k'_A, defined in Eq. (7), of 3×10^{-6} was selected so as to provide an approximate fit to the data. When Eq. (3) with k_D defined by Eq. (32) is applied to data in vertical pipes a value $k'_A = 1.4\times10^{-6}$ is obtained. This is smaller than the value of 3×10^{-6} needed to fit the data in Fig. 7. This should not be surprising since the use of the equation for vertical flows to represent local values of R_A in horizontal flows is only an approximation.

Fig. 7(a) used Eq. (25) to calculate d_{32}; i.e., d_{32} is dependent on pipe diameter. The calculations for $D = 9.53$ cm are below the calculations for $D = 2.31$ cm at low U_G and above them at high U_G. The calculated E/E_M are larger for $D = 9.53$ cm than for $D = 2.31$ cm for all gas velocities.

The important result is that the theoretical calculations show a smooth transition between low and high velocity behaviors for which $(E/E_M)/1-(E/E_M)$ varies roughly as U_G^5 and U_G^2. One is characteristic of a system in which gravitational settling is controlling deposition. The other is characteristic of a vertical flow. The theoretical curves capture the behaviors in the pipes with $D = 2.31$ cm and $D = 5.08$ cm reasonably well. However, the theoretical curve for $D = 9.51$ cm lies to the left of the measurements. This difference is within the range of errors that would result from predicting drop size and the concentration profiles of the drops.

The measurements in Fig. 7 were made under conditions that the influence of gravitational settling was strong. Consequently, comparisons of the calculations and the experiments at large U_G are inconclusive. As mentioned above the predicted influence of U_G on $(E/E_M)/1-(E/E_M)$ is what is expected for vertical flows. However, measurements in vertical flows lie below these predictions. This suggests that data at large U_G could go through a maximum before they reach a condition where the behavior is the same as for vertical annular flow. However, these considerations might not be of importance since the differences in $(E/E_M)/1-(E/E_M)$ translate into small differences in E/E_M where E is large.

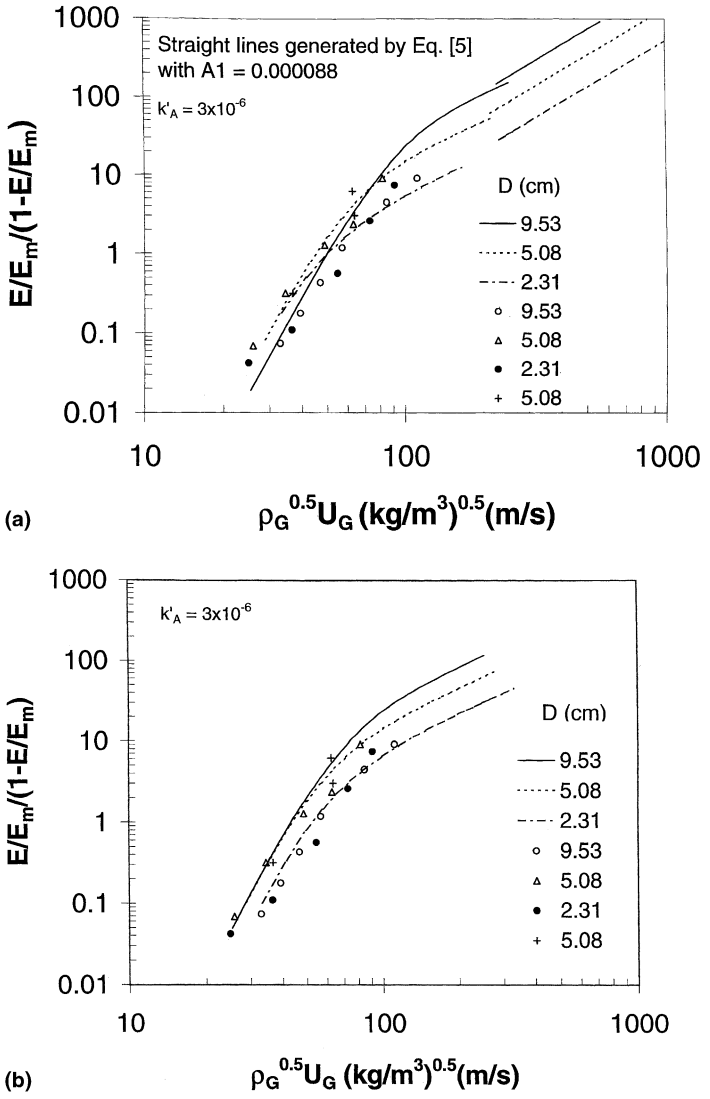

Fig. 7. Calculations of $(E/E_M)/1-(E/E_M)$ using Eq. (13) with $k'_A = 3 \times 10^{-6}$: (a) drop size, d_{32} calculated with Eq. (25); (b) d_{32} calculated with Eq. (26).

6. Calculations for a natural gas

This section explores how the correlation developed from data for air and water flowing in a horizontal pipe can be used to represent the behavior of a natural gas pipeline. Table 3 summarizes system variables used in the Bacton experiments carried out by Shell (Wu et al., 1987). The ranges of u_T/σ_p for the natural gas pipeline, in the annular flow regime are 0.02–0.5. This is to be compared with u_T/σ_p of 0.25–2.5 for air–water flow in a 9.53 cm pipe.

Table 3
Conditions in a natural gas pipeline

D (m)	0.2032
ρ_G (kg/m^3)	65
Pressure (bar)	75
ρ_L (kg/m^3)	720
μ_G (mPa s)	1×10^{-5}
μ_L (mPa s)	0. 00055
σ (N/m)	0. 0118

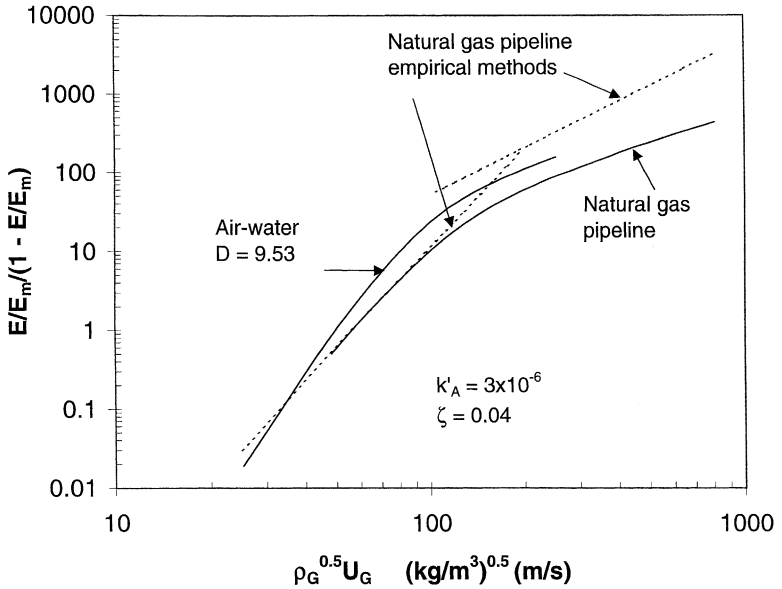

Fig. 8. Calculations of $(E/E_M)/1-(E/E_M)$ for a natural gas pipeline are compared with air–water flow in a 9.53 cm pipe – the solid curves. The dashed lines represent calculations for a natural gas pipeline using empirical relations, Eqs. (18) and (5). Eq. (25) is used to calculate d_{32}.

Fig. 8 presents the calculated values of $(E/E_M/1-E/E_M)$ over a range of $\rho_G^{0.5}U_G$ where annular flow existed. The droplet concentration profiles were obtained with Eq. (53) and d_{32}, with Eq. (25). The eddy diffusivity was given by $\varepsilon = 0.04(D/2)v^*$ for both the natural gas and the air–water systems. The atomization constant, $k'_A = 3 \times 10^{-6}$, is the same as determined in Section 5.

An alternate approach is to use empirical equation (18) with $A_2 = 9 \times 10^{-8}$ to represent the behavior of the natural gas pipeline at low gas velocities and empirical equation (5) with $A_1 = 8.8 \times 10^{-5}$ to represent the behavior at large gas velocities. These relations are also plotted in Fig. 8. Good agreement between the empirical and analytical approaches is noted at low U_G. However, Eq. (5) predicts larger entrainments than are obtained with the analysis.

Calculated plots of E versus W_L are presented in Fig. 9, where values of E/E_M from the analytical solution were used to construct the solid curves. The dashed curves represent calculations that use E/E_M from the empirical correlations, Eqs. (18) and (5).

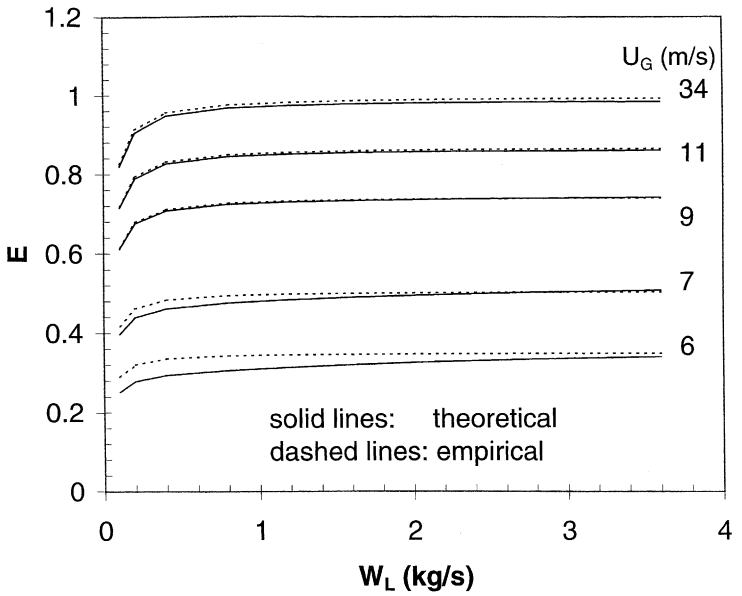

Fig. 9. Plots of E for a natural gas pipeline. The solid curves use the analytical equations. The dashed curves were obtained from the empirical relations, Eqs. (18) and (5) for E/E_M.

Fig. 8 indicates that the substitution of $k_D/S = U_G$ into Eq. (3) to obtain Eq. (5) is an oversimplification since k_D/U_G is not a constant. The value of $A_1 = 8.8 \times 10^{-5}$ was obtained from calculations for the air–water flows represented in Fig. 7. A smaller A_1 is needed to represent a natural gas pipeline. A better approach would be to use Eq. (32) to calculate k_D for vertical flows. However, for the case considered, the errors in calculating the asymptotic values of $(E/E_M)/1 - (E/E_M)$ for large U_G do not translate into large errors in E, as seen in Fig. 9.

The predictions in Figs. 8 and 9 depend on the choice of an equation for d_{32}. Somewhat different results would be obtained if Eq. (26) were used, instead of Eq. (25).

7. Discussion

This paper uses a limited amount of data to develop a relation for entrainment, under fully developed conditions, when the liquid viscosity is close to that of water. The approach is to define entrainment as a balance between the rates of atomization and deposition. The influence of fluid properties on R_A is determined from experiments on flow in vertical pipes with small diameters. The behavior of the horizontal system is determined from experiments with air and water at conditions close to those that prevail in the atmosphere. If $U_G/(gD)^{0.5}$ is small, gravitational settling will play a dominant role in determining the deposition rate. At very high $U_G/(gD)^{0.5}$, gravity becomes an unimportant factor so that the behavior will be close to what is observed for a vertical pipe.

The practice of using correlations for vertical annular flows to predict entrainment in horizontal configurations is flawed because the range of gas velocities where E changes from zero to a value

close to unity is usually characterized by small $U_G/(gD)^{0.5}$. The contribution of this paper is that it presents methods (perhaps, for the first time), for correlating measurements, which directly account for the influence of gravitational settling. Two approaches are explored:

1. Empirical relations for the entrainment in horizontal pipes at low U_G and for vertical pipes at high U_G are used.
2. A theoretical analysis of particle turbulence is used to obtain a general relation for R_D which is valid both for large and small $U_G/(gD)^{0.5}$.

An important simplifying assumption is that the influence of liquid flow is introduced only in the definition of E_M. Thus, equations for R_A and R_D which are strictly valid only for small W_L are used. The justification for this approach is the observation that E/E_M is much more sensitive to changes in U_G than to changes in W_L. The influences of W_L, such as shown in Fig. 1, are not considered. Instead, measurements of E/E_M for different W_L, at a fixed U_G, are averaged. These $\langle E/E_M \rangle$ are then used to test correlations that are developed.

The empirical approach involves the use of Eq. (18) with $A_2 = 9 \times 10^8$ to calculate E at small U_G and Eq. (3) with $k_D = (\sigma_p^2/2\pi)^{0.5}$, $k'_A = 3 \times 10^{-6}$ at large U_G. Another less accurate way of representing the behavior at large U_G is to use Eq. (5) with $A_1 = 8.8 \times 10^{-5}$. The important finding in comparing this approach with experimental results is that it correctly captures the influence of U_G on the measurements of E/E_M. However, it is less successful in capturing the effect pipe diameter (and, perhaps, ρ_G) because of uncertainties in specifying the drop diameter and because the influence of asymmetries on the spatial distribution of the liquid is not directly taken into account in Eq. (18).

Nevertheless Eq. (18) provides a good first approximation for the entrainment (particularly if reliable measurements for drop size become available). An improved empirical correlation is suggested which uses the critical gas velocity, U_{GC}, for the initiation of annular-dispersed flow and Eq. (23) with $d \sim U_G^{-1}$. Thus, if U_{GC} is defined as the gas velocity for which $(E/E_M)/1 - (E/E_M)$ equals some small number, say 0.05, the following equation is developed:

$$\frac{E/E_M}{1-(E/E_M)} = 0.05\left(\frac{U_G}{U_{GC}}\right)^3\left(\frac{U_G}{U_{GC}}\right)^{(1+m)/(2-m)}. \tag{58}$$

A correlation for U_{GC} would then provide a definition of the influence of pipe diameter and fluid properties.

The analytical approach uses Eq. (13) with $k'_A = 3 \times 10^{-6}$ and $\langle k_D C_W/C_B \rangle$ specified as the products of V_W, given by Eq. (31), and C_W/C_B, given by Eq. (53). This provides a theoretical description of how the behavior of E/E_M changes from one in which gravitational settling controls, to one in which particle turbulence controls the rate of deposition. The implementation of this theory is handicapped because of the sparcity of measurements of drop size, because of the need for an improved theoretical analysis of how drops distribute in the gas phase and because of the sparcity of measurements of entrainment in horizontal pipes. Nevertheless, the analysis should provide a good first approximation for entrainment in horizontal flows for liquids

whose viscosity is close to that of water – and a better approximation when more data become available.

Acknowledgements

This work was supported by the Energy Research Program of the Office of Basic Energy Sciences at the Department of Energy under grant DOE DEF G02-85ER-13556 and by Shell Technology.

References

Andreussi, P., Asali, J., Hanratty, T.J., 1985. Initiation of roll waves in gas–liquid flows. AIChE J. 31, 126.

Assad, A., Jan, C.S., Lopez de Bertodano, M., Beuss, S., 1998. Scaled entrainment measurements in ripple–annular flow in a small tube. Nucl. Eng. Des. 184, 443–446.

Azzopardi, B.J., 1985. Drop sizes in annular two-phase flow. Exp. Fluids 3, 53–59.

Cousins, L.B., Denton, W.H., Hewitt, G.E., 1965. Liquid mass transfer in annular two-phase flow. Paper presented at the Symp. on Two-Phase Flow, Exeter, UK, 21–23 June.

Dallman, J.C., 1978. Investigation of separated flow model in annular gas–liquid two-phase flows. Ph.D. Thesis, University of Illinois, Urbana.

Dallman, J.C., Jones, B.G., Hanratty, T.J., 1979. Interpretation of entrainment measurements in annular gas–liquid flows. In: Durst, F., Tsiklauri, G.V., Afgan, N.H. (Eds.), Two-Phase Momentum, Heat and Mass Transfer, vol. 2. Hemisphere, Washington, DC, pp. 681–693.

Dallman, J.C., Laurinat, J.E., Hanratty, T.J., 1984. Entrainment for horizontal annular gas–liquid flow. Int. J. Multiphase Flow 10, 677–690.

Dykhno, L.A., Williams, L.R., Hanratty, T.J., 1994. Maps of mean gas velocity for stratified flow with and without atomization. Int. J. Multiphase Flow 20, 691–702.

Hanratty, T.J., Woods, B.C., Iliopoulos, I., 2000. The roles of interfacial stability and particle dynamics in multiphase flows; a personal viewpoint. Int. J. Multiphase Flow 26, 169–190.

Hay, K.J., Liu, Z.C., Hanratty, T.J., 1996. Relation of deposition to drop size when the rate law is nonlinear. Int. J. Multiphase Flow 22, 829–848.

Hoogendorn, C.J., Welling, W.A., 1979. Experimental studies on the characteristics of annular-mist flow in horizontal pipes. In: Durst, F., Tsiklauri, G.V., Afgan, N.H. (Eds.), Two-Phase Flow Momentum, Heat and Mass Transfer, vol. 2. Hemisphere, Washington, DC, pp. 301–310.

Laurinat, J.E., 1982. Studies of the effects of pipe size on horizontal annular two-phase flows. Ph.D. Thesis, University of Illinois, Urbana.

Laurinat, J.E., Hanratty, T.J., Dallman, J.C., 1984. Pressure drop and film height measurements for annular gas–liquid flow. Int. J. Multiphase Flow 10, 341–356.

Lee, M.M., Hanratty, T.J., Adrian, R.J., 1989a. The interpretation of droplet deposition measurements with a diffusion model. Int. J. Multiphase Flow 15, 459–469.

Lee, M.M., Hanratty, T.J., Adrian, R.J., 1989b. An axial viewing photographic technique to study turbulence characteristics of particles. Int. J. Multiphase Flow 15, 787–802.

Lopez de Bertodano, M.A., Assad, A., 1997. Entrainment rate of droplets in the ripple–annular regime for small diameter vertical ducts. In: Third Internat. Conf. on Multiphase Flow, Lyon, France.

Lopez de Bertodano, M.A., Jan, C.S., Beuss, S.G., 1994. Annular flow entrainment rate experimental in a small vertical pipe. Nucl. Eng. Des. 178, 61–70.

Mugele, R., Evans, H.D., 1951. Droplet size distribution in sprays. Ind. Eng. Chem. 43, 1317–1324.

Paras, S.V., Karabelas, A.L., 1991. Droplet entrainment and deposition in horizontal annular flow. Int. J. Multiphase Flow 17, 455–468.

Schadel, S.A., Leman, G.W., Binder, J.L., Hanratty, T.J., 1990. Rates of atomization and deposition in vertical annular flow. Int. J. Multiphase Flow 16, 363–374.

Tatterson, D.F., Dallman, J.C., Hanratty, T.J., 1977. Drop sizes in annular gas–liquid flows. AIChE J. 23, 68–76.

Wicks, M., Dukler, A.E., 1960. Entrainment and pressure drop in concurrent gas-liquid flow: air–water in horizontal flow. AIChE J. 6, 463–480.

Williams, L.R., 1986. Entrainment measurements in a 4-inch horizontal tube. M.S. Thesis, University of Illinois, Urbana.

Williams, L.R., 1990. Effect of pipe diameter on horizontal annular two-phase flow. Ph.D. Thesis, University of Illinois, Urbana.

Williams, L.R., Dykhno, L.A., Hanratty, T.J., 1996. Droplet flux distributions and entrainment in horizontal gas–liquid flows. Int. J. Multiphase Flow 22, 1–18.

Wu, H.L., Pots, B.F.M., Hollenburg, J.F.S., Meerhof, R., 1987. Flow pattern transition in two-phase gas/condensate flow at high pressure in an 8-inch horizontal pipe. In: Proc. BHRA Conf., The Hague, The Netherlands, pp. 13–21.